International Journal of Heat and Mass Transfer 107 (2017) 736–746

Contents lists available at ScienceDirect

International Journal of Heat and Mass Transfer

journal homepage: www.elsevier.com/locate/ijhmt

Effective gas diffusion coefficient in fibrous materials by mesoscopic modeling

Xinting He [a,1], Yangyu Guo [a,1], Min Li [c], Ning Pan [b], Moran Wang [a,*]

[a] Department of Engineering Mechanics and CNMM, Tsinghua University, Beijing 100084, China
[b] Biological and Agricultural Engineering, University of California at Davis, CA 95616, USA
[c] State Key Laboratory of Oil and Gas Reservoir Geology and Exploitation, Southwest Petroleum University, Chengdu, China

ARTICLE INFO

Article history:
Received 19 July 2016
Accepted 27 November 2016
Available online 7 December 2016

Keywords:
Effective diffusion coefficient
Fibrous material
Lattice Boltzmann method
Mesoscopic modeling

ABSTRACT

This paper presents a method to establish a relationship between internal microstructure and the effective gas diffusion coefficient in fibrous materials via a mesoscopic modeling approach and, when possible and based on the analysis, to propose user-friendly formulas as functions of structural parameters for practical engineering applications. The entire numerical framework includes two main parts: a random generation-growth method to reconstruct the digital microstructures of fibrous materials based on experimental statistical information of the actual structure, and then a high-efficiency lattice Boltzmann algorithm for modeling the gas diffusion process through porous structures. The predictions are then validated by existing experimental data for both dry and saturated fibrous materials. Owing to the unique robustness of the developed modeling approaches, we are then able to conduct a parametric analysis, more detailed than ever, of the influences on the system effective diffusion coefficient in fibrous materials by such important parameters as structural anisotropy, system water content, microstructure morphology and the layering space in a laminated fibrous system. These results may improve our understanding of gas diffusion in fibrous materials, and this method may serve as a tool for easy estimation of effective diffusivity, leading to the optimal design of fibrous materials.

1. Introduction

Diffusion of a substance in another media is a spontaneous movement of the substance caused by its concentration gradient, and governed by Fick's laws of diffusion, or at a microscopic view, as the random walk of the diffusing particles self-propelled by thermal energy [1]. The most unique characteristics in diffusion are the small length scale concerned, limited in between micrometer and millimeter, and the trifling amount of mass involved [1]. Such characteristics of transporting mass in tiny amount over minor spatial scale render the diffusion process less visible, but fundamentally essential and ubiquitous in many physical, chemical phenomena and beyond. In fact, the process of diffusion is so prevalent that, together with reaction, it was considered the "possible basis of modern micro- and nanotechnologies" [2]. What is more vital, at such minuscule spatial scale, the interfacial effects become much more dominant in determining the system properties.

For practical applications, a thorough understanding of the mechanisms involved in a given diffusion process is crucial for design and optimization. For instance, gas diffusion in fibrous materials, one of the common occurrences such as mass transport through fibrous screen filters in many filtering processes, and through gas diffusion layer (GDL) in fuel cells, is considered essential in many engineering fields [3–5]. A deep understanding of how the fibrous microstructures affect the diffusive flux can lead to significant improvements in product design [6]. Macroscopically a porous medium by definition is a two-phase (solid and air) system, and the gas diffusion efficacy in porous media is usually considered a function of the system porosity ε, the internal tortuosity τ, and the pore size distributions [6], and has been widely studied via theoretical, experimental and numerical methods [7–11]. Below we will present a very brief overview of previous work on diffusion in fibrous materials in terms of these different methods respectively.

In theoretical aspect, both deterministic modeling based on Fick's diffusion equation, and stochastic approaches rooted in random walk picture have been widely applied to investigate various

* Corresponding author.
E-mail addresses: npan@ucdavis.edu (N. Pan), mrwang@tsinghua.edu.cn (M. Wang).
[1] The first two authors contribute equally to this work.

http://dx.doi.org/10.1016/j.ijheatmasstransfer.2016.11.097
0017-9310/

diffusion processes. Several studies have recommended different models to predict the behaviors of gas diffusion through fibrous materials. For instance, the simplest model is proposed by assuming a fibrous material as the assembly of a bundle of tortuous channels, and demonstrated in a normalized form that the effective diffusivity is related to the bulk diffusivity in the void in terms of both porosity and tortuosity. Although the porosity here is easy to be calculated or measured, the practical applicability of this model is crippled by the difficulty in accurately determining the value of tortuosity. Bruggeman [12] also presented a model based on the effective medium approximation. However, this model was derived from a system with uniformly packed spherical particles rather than media with more intricate internal structures. Li et al. [13] treated a fibrous material as a system formed by cylindrical fibers arranged either in square or hexagonal configuration. Then by varying the width of the gap between fibers, the effect of the system porosity was investigated. Their model however over-predicted the material diffusivity, and one possible cause is that the gas concentration was assumed in their analysis to be constant at any cross-section of the material. Recently, Shou et al. [14] proposed a fractal model for gas diffusion through nanofibrous and microfibrous materials including both the Fick's diffusion and Knudsen diffusion. However, too many simplifications were made such as the pores in fibrous media form a bundle of tortuous open channels with statistically fractal-like sizes. Thus this fractal model remains to be validated by experimental data in more different fibrous structures beyond the specific highly anisotropic nanofibrous webs and GDLs considered in their work.

Experimentally, the effective diffusivity of fibrous materials as defined can be determined in principle by measuring the diffusive flux and the directional concentration gradient. Penman [7] measured the cross-plane diffusion coefficient of a steel wool sample as early as in 1940. In a similar way, Bateman et al. [15] obtained the effective diffusivity of NO gas penetrating through a 2D cellulosic filter. Gibson et al. [16] used a dynamic diffusion test cell method to measure the effective diffusivity of vapor in fibrous media by getting the change of relative humidity in the vapor. The dynamic diffusion cell is also used by LaManna and Kandlikar [17] to investigate the effects of micro-porous layer (MPL) coatings and sample thickness on the effective water vapor diffusion coefficient in GDLs.

In terms of computational simulation and numerical approaches, owing to the rapid development of computational techniques, a variety of major numerical schemes have been developed for analyzing the mass transport in fibrous media. The single component gas flow and effective permeability in fibrous materials has been widely studied usually by combining stochastic method for structure generation and highly efficiency numerical schemes like the lattice Boltzmann method [18,19]. In contrast, there is much less work on the gas diffusion in fibrous structures as another important mass transport process. Tomadakis and Sotirchos [20] used Monte Carlo method to simulate gas diffusion in 1D, 2D and 3D regular fiber networks and calculated the effective diffusivity. Becker et al. [21] numerically reconstructed a fibrous structure from a 3D image, and then developed a relationship between the effective diffusion coefficient and the saturation of the GDL. Zamel et al. [22] used GeoDict software to generate the structure of a carbon paper, and imported the structure into a commercial CFD to compute the effective diffusion coefficient of fibrous media.

However, a review of the existing work uncovers that most of the previous studies focus on specific and regular microstructures of the media, ignoring the structural variations and the intricate system geometries. For instance, in a fibrous media of given porosity, when parameters like fiber size and orientation vary, it can give rise to vastly different internal porous structures and hence diverse diffusion behaviors. A general approach dealing with the diffusive physics in fibrous materials as a whole, i.e., demonstrating the effects of fiber and structure parameters on the system effective diffusion coefficient is highly desirable, yet non-existent to our best knowledge; this therefore becomes the main objective of this present work. It will be shown at the end that attributed to the unique robustness of our new modeling approaches, we are able to investigate, more detailed than ever, the influences on the system effective diffusion coefficient in fibrous materials of such important parameters as the fiber orientation hence the structural anisotropies, system water content, microstructure morphology and the layering space in a laminated fibrous system.

This article is organized as follows: In Section 2, we introduce the theoretical foundation and numerical framework of our approach, including a random generation growth method for microstructure reproduction for fibrous, granular as well as partially saturated porous media; the governing equations for gas diffusion; and a lattice Boltzmann solver for the governing equations. In Section 3, the present method is validated with existing theoretical solutions and experimental data from other publications. Then in Section 4, the structure effects (liquid saturation, types of structures, orientation angle of fiber, and the layer-spacing in a laminated structure) on gas diffusion in porous media are analyzed. Concluding remarks based on this study are finally made in Section 5.

2. Numerical framework

2.1. Reconstruction of microstructures

To study the microstructure effect via computational modeling, we have to reconstruct the microstructures of porous materials in the computer. Generally speaking, the microstructures of actual porous media have some significant features, often being stochastic with statistical characteristics and rarely if ever regular and remaining constant. To photo-realistically reproduce the intricate details of such microstructures is both impractical and unnecessary. In fact, if our interest is on the steady state as in this case of fluid diffusion, the macroscopic (effective) transport properties of such systems are actually governed by the statistical average values of the parameters involved. As a result, we adopt a multi-parameter random generation-growth algorithm to reconstruct the random microstructures using the statistical average information from the real porous materials [23,24]. The equivalent structure generated this way with finite parameters will reflect the major characteristics of the actual system. The another major issue in tackling such porous media is the morphological difference, and different morphologies have demonstrated very significant impact on the effective energy transport properties, such as on thermal conductivity [25]. Microstructures of porous media may be roughly divided into three categories in morphology: fibrous, granular and network structures [25]; we hence designed the reconstruction methods for each type correspondingly. To consider the liquid saturation effect when water coexists in a system, an algorithm describing the multiphase distributions will be presented, as detailed in the following paragraphs.

For a fibrous structure, the algorithm assumes that each fiber is represented by a straight cylinder with given diameter d and length l, and located by its core position (the geometrical center) and an orientation angle pair (ϕ,θ) as shown in Fig. 1 [26]. When describing the size of a fiber, fiber aspect ratio $p = l/d$ is often used, as also in this work, and a larger p value represents a slenderer shape (longer length or thinner diameter). The generation process for a three dimensional fibrous microstructure is conducted as follows: (***i***) randomly distributing fiber seeds (center) in a given grid system based on the seed distribution probability s_d, whose value is determined by the fiber number density; (***ii***) assigning a random

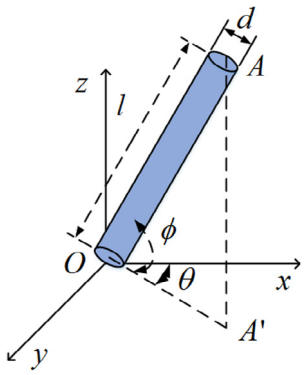

Fig. 1. Schematic of a fiber oriented in a three dimensional space. The fiber is represented by a straight cylinder OA with a diameter d and length l. A′ is the projection of A on $x-y$ plane. (ϕ, θ) is the orientation angle pair of the fiber OA.

numbers pair to the orientation angles (ϕ,θ) for each seeds to define the fiber orientation. For isotropic materials, the orientation angles can be any values within 0~2π randomly; (***iii***) then extending (growing) the length of each fiber from both ends along the direction of (ϕ,θ); (***iv***) terminating the fiber growth process upon fiber length meeting the given value, or the system porosity reaching the prescribed value, whichever comes first [24,26].

For granular structures, our multi-parameter random generation-growth method, referred as QSGS [23,27], includes five steps: (***i***) in a grid system, assigning each cell a random number using a uniform distribution function within (0, 1); (***ii***) choosing any cell whose random number is no greater than a given threshold s_d as a seed; (***iii***) enlarging (growing) each seed to its neighboring cells in all directions i based on a given directional growth probability matrix D_i; (***iv***) assigning random numbers again to the neighboring cells of the grown seed, the neighboring cell in direction i will become part of the growing solid phase by merging with the grown seed if its random number is no greater than D_i; (***v***) repeating the growing process of (***ii***)–(***iv***) until the volume fraction of the solid phase reaches its presubscribed value.

Fig. 2(a), (b) and (c) demonstrate the 3D view of granular, isotropic fibrous and multiplayer fibrous structure generated by the above growth methods, respectively.

For systems with more than two phases, for instance, a system with solid, air and liquid, the additional liquid phase can be regenerated in a similar way [28]. The solid phase is generally selected as the first growing phase, the liquid phase will grow on solid surfaces or the existing liquid surfaces, and air finally fills the space left. The liquid phase growth depends on two phase interaction growth probability matrix: $I_i^{l,s}$ and $I_i^{l,l}$, which represents the growth probability of the liquid phase l on the solid surface s or on the existing liquid surface, respectively, along the i-th direction. Below are the steps of liquid phase growth: (***i***) selecting potential liquid phase seeds randomly on the solid surfaces which have been pre-divided into grid and each cell will be designated a random number within (0, 1), then those with number no greater than corresponding probability $I_i^{l,s}$ will be chosen as the actual seeds for liquid phase; (***ii***) growing the liquid seed on the solid surface $I_i^{l,s}$ or on the liquid surface whichever probabilities $I_i^{l,s}$ and $I_i^{l,l}$ is greater; (***iii***) repeating the growing process in (***ii***) until the liquid phase reaching its given saturation value. Fig. 3 shows the 3D morphologies thus generated of granular and fibrous systems with partial saturation.

2.2. Governing equations

The diffusion coefficient of a gas is a function of among other things the gas concentration, temperature, and pressure [29]. Here we consider a simple binary gas diffusion process through a three-dimensional fibrous porous structure. The mathematical models for gas diffusion are generally under the following assumptions: (***i***) the entire system is in dynamical equilibrium, where advection is negligible; (***ii***) the diffusion process is in steady state; (***iii***) the temperature and total pressure of the environment remain constant, and the gas concentration is low; (***iv***) the pore size is sufficiently larger than the mean free path of gas molecules; (***v***) although the pore size is at the order of microns, the gas at the ambient temperature and pressure can still be treated as a *continuum* medium, i.e., following the Newtonian fluid assumption and the Fick's law.

The governing equation for the gas diffusion in fibrous media is as follows [29]:

$$\nabla \cdot (D_b \nabla C) = 0, \tag{1}$$

with the boundary conditions:

$$\begin{aligned} C(x,y,z) &= C_{in}, x = 0 \\ C(x,y,z) &= C_{out}, x = L \end{aligned} \tag{2}$$

where D_b represents the bulk diffusivity of the gas, C is the gas concentration. As is shown in Fig. 4, a certain yet constant concentration gradient along x-axis was produced: $\Delta C = C_{in} - C_{out}$ over the boundaries located at $x = 0$ and $x = L$, and other boundaries were considered as periodic boundary conditions.

2.3. Lattice Boltzmann method

Applying Eqs. (1) and (2) for gas diffusion in the porous structure generated, we use an efficient lattice Boltzmann method (LBM) to solve the equations in such complex geometries [24,30]. For such cases, the corresponding lattice evolution equation can be expressed as [31]:

$$g_\alpha(\mathbf{r} + \mathbf{e}_\alpha \delta_t, t + \delta_t) - g_\alpha(\mathbf{r}, t) = -\frac{1}{\tau_n}\left[g_\alpha(\mathbf{r}, t) - g_\alpha^{eq}(\mathbf{r}, t)\right] \tag{3}$$

where g_α^{eq} is the local equilibrium distribution in each direction α, and $\mathbf{e}_\alpha$ denotes the discrete lattice velocities for a three-dimensional seven-speed (D3Q7) system shown in Fig. 5, τ_n the dimensionless relaxation time for the local phase.

The equilibrium distribution of the evolution variable g_α, for the D3Q7 model is related to the local gas concentration:

$$g_\alpha^{eq} = \begin{cases} \frac{C}{4} & \alpha = 0 \\ \frac{C}{8} & \alpha = 1-6 \end{cases}, \tag{4}$$

the discrete lattice velocities are fully expressed as:

$$\mathbf{e}_\alpha = \begin{cases} (0,0,0) & \alpha = 0 \\ (\pm 1,0,0)c, \quad (0,\pm 1,0)c, \quad (0,0,\pm 1)c & \alpha = 1-6 \end{cases} \tag{5}$$

and the dimensionless relaxation time is related to the gas transport coefficient:

$$\tau_n = \frac{1}{2} + \frac{4D_b}{c^2 \delta_t} \tag{6}$$

where δ_t is the time step, $D_b$is the bulk diffusivity of gas, and c is the lattice speed.

Based on the solution of the evolution variable at mesoscale, the macroscopic local concentration and mass diffusive flux can be calculated through statistical process [32]:

$$C = \sum_\alpha g_\alpha, \tag{7}$$

$$J = \frac{(\tau_n - 0.5)}{\tau_n} \sum_\alpha g_\alpha \mathbf{e}_\alpha. \tag{8}$$

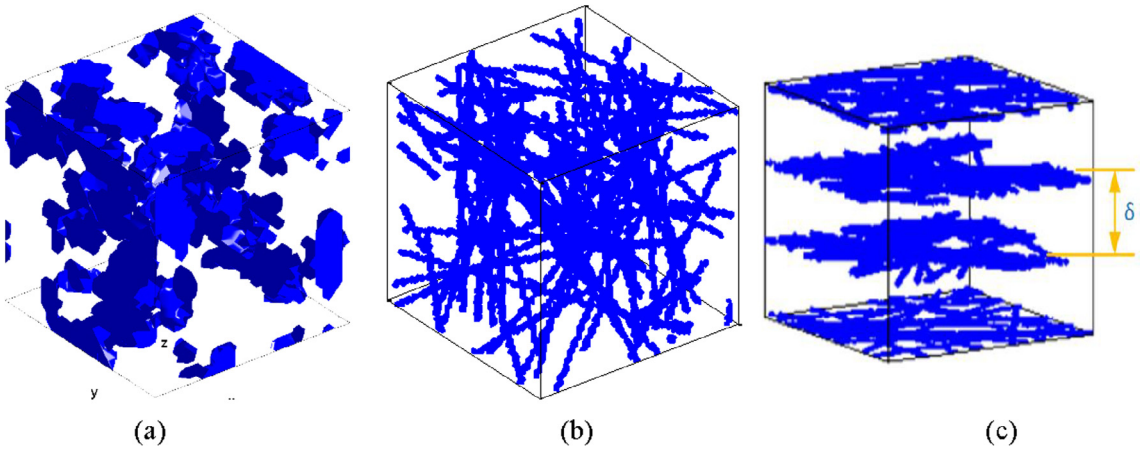

Fig. 2. Schematic of reproduced porous structures: (a) granular (b) isotropic fibrous (c) multi-layer fibrous. For the sake of schematic simplicity, a layer-spacing parameter (δ) is used to characterize the multiplayer structure.

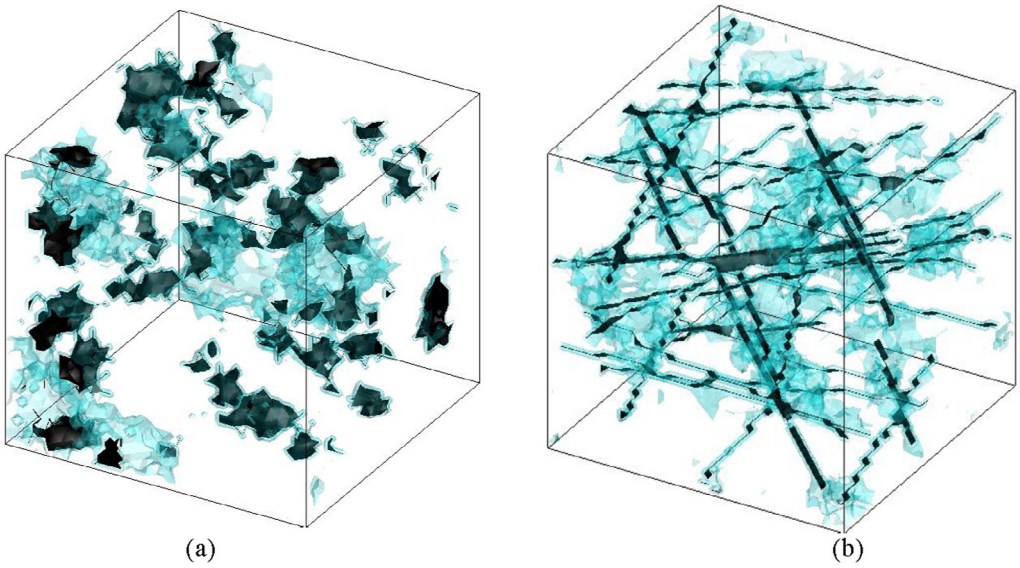

Fig. 3. Schematic of partially saturated microstructures of (a) granular and (b) fibrous porous media. The black is the solid frame and the blue represents the liquid phase.

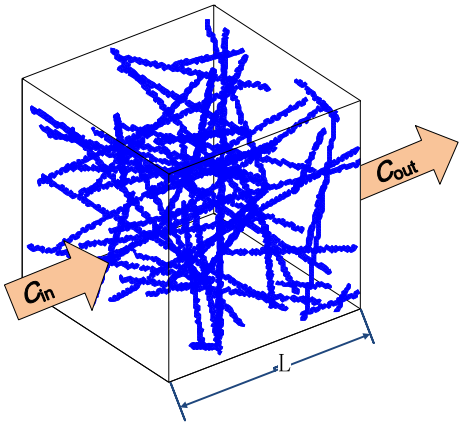

Fig. 4. Schematic for diffusion in cubic porous medium. The cube is L in length. The concentrations of inlet and outlet are given as C_{in} and C_{out}, respectively.

Once the mass diffusion is solved, the effective diffusion coefficient can be obtained based on the Fick's law [23]:

$$D_e = \frac{L \int J dA}{\Delta C \int dA}. \quad (9)$$

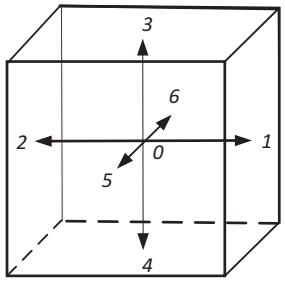

Fig. 5. The D3Q7 lattice strucuture in lattice Boltzmann method.

In terms of the boundary condition treatments on the solid walls, the traditional bounce-back rule is used due to its high efficiency in complex geometries. The non-equilibrium bounce-back rule [33] is adapted for the concentration boundaries, i.e. $g_{\alpha}^{neq} = g_{\beta}^{neq}$, with the subscripts α and β representing two opposite directions. It has been proved that such boundary treatments have an approximately second-order accuracy [33]. After considering the solution stability, numerical accuracy and grid independence, an $80 \times 80 \times 80$ lattice system was used as the computational domain except the benchmark in Section 3.1. In addition, we have

checked that the exact morphology of the porous materials under the same statistical parameters used for reconstruction has negligible effect on the results of effective diffusion coefficient.

3. Validations

To validate the present methods in predicting the effective diffusion coefficient in fibrous materials, this section compares our numerical results with the existing theoretical solutions and/or experimental data as follows.

3.1. Comparison with theoretical solution

First we consider a simple one-dimensional transient gas diffusion process through a blank region as shown in Fig. 6(a). The gas concentrations at left and right boundaries over a distance L are given. The initial state is a uniform gas concentration of C_2 throughout the domain. At time t=0, the gas concentration on the left boundary is suddenly increased to C_1. Throughout the present work, we consider the diffusion of air through the system at room temperature with a bulk diffusivity $D_b = 4 \times 10^{-4} m^2/s$. Assuming no internal concentration source and constant material diffusivity, the mathematical description of this one-dimensional diffusion is as follows:

$$\frac{\partial C}{\partial t} = D_b \frac{\partial^2 C}{\partial x^2}, \tag{10}$$

$$\begin{aligned} &C = C_2, 0 < x < L, t = 0 \\ &C = C_1, x = 0 \\ &C = C_2, x = L \end{aligned} \tag{11}$$

By introducing the dimensionless spatial and temporal coordinates as: $X = x/L$ and $Fo = D_b t/L^2$, one can obtain the series analytical solution for such a problem by the method of variable separation [34]:

$$\Theta = \frac{C(x,t) - C_2}{C_1 - C_2} = 1 - X - \frac{2}{\pi}\sum_{n=1}^{\infty} \frac{\sin(n\pi X)}{n} \exp\left[-(n\pi)^2 Fo\right] \tag{12}$$

The computational domain in this case was divided into a 400×40×4 grid, with a lattice spatial step 1 μm for LBM modeling. x-Direction is assumed the concentration boundary whereas both y- and z-directions are assumed the periodic ones. Fig. 6(b) compares the distribution of dimensionless gas concentration (Θ) along the diffusion path at different dimensionless instants (Fo). Appreciably good agreements are seen between them, confirming the feasibility and reliability of our LBM codes.

3.2. Comparisons with experimental data for granular structures

To compare with the experimental data from literature, we first use our reconstruction algorithm to generate the corresponding microstructures and then calculate the effective gas diffusion coefficient of the system with prescribed boundary conditions via our LBM model. Since granular porous media have been studied extensively for their broad engineering applications with more available experimental data, we hence focus on such systems first in this section. The system porosity in the present numerical prediction is consistent with that of experimental material. For the seed distribution probability, after verifying the numerical results are insensitive to its value, we adopt a typical value of $s_d = 0.01$ from previous literature [23] in reconstructing the granular material. The details of the directional growth probability matrix D_i could be found in our previous work [23]. After the local concentration and mass flux are evaluated through a statistical summation of the lattice evolution function via Eqs. (7) and (8), the effective gas diffusivity is then extracted from an integration of the local mass flux along an arbitrary cross-section perpendicular to the transport direction based on Eq. (9). The effective gas diffusivity in other porous structures is obtained through a similar procedure.

Fig. 7 shows the comparison of the effective gas diffusion coefficient between our present predictions and the experimental data for granular structure [35–37]. Generally, the pore size in soils is larger than the mean free path of gas, thus the gas diffusion behavior in soils is close to obey the Fick's law. In Ikkonen's work [35], we discarded the data from top layer for fear of less stable structure, and only used data of the three deeper layers for comparison. The highly agreeable results are seen in the figure. We also made other comparisons in Fig. 7 with the data from two additional experimental sources [36,37] on soils and some other media whose microstructures could belong to the granular types. Again our predictions agree well with the experimental results, demonstrating a robust capacity of our numerical approach.

It was interesting to find a recent work [38] which, using virtually the similar reconstruction algorithm and LBM model, predicted results in good agreement with Currie's data [37]. There are though some differences between their LBM model and the present one introduced in Section 2.3. The lattice Boltzmann scheme in Ref. [38] is developed from the kinetic transport equation for binary diffusion, and involves an evolution of two distribution functions; in contrast, we adopt a simpler single lattice evolution equation Eq. (3), which recovers exactly the Fick's law of diffusion through Chapman-Enskog expansion. On the other hand, a D3Q19 lattice structure has been used in Ref. [38] whereas we chose the D3Q7 lattice structure to avoid the unphysical oscillation near the boundary throughout numerical solution. In terms of the computed system effective diffusivity versus the porosity, a closer examination revealed that their predicted curve showed some unexpected non-smoothness i.e., a zigzag rather than a smooth curve. One possible cause may be the inconsistent parameters used in their work when reconstructing the microstructures for different porosities, since in principle such sudden changes in system macro-behaviors are difficult to explain. In the present work we use consistent statistical parameters, including s_d and D_i, in microstructure reconstructions for variable porosities. Therefore we achieve a smooth variation of effective gas diffusion coefficient versus the system porosity as seen in Fig. 7.

3.3. Comparisons with experimental data for fibrous structures

Attributed to their unique advantages, more and more fibrous structures are found playing key roles in energy and environmental systems. For example, random fibrous materials, saturated or unsaturated, have been used in fuel cells to facilitate the gas diffusion performance in the gas diffuse layer (GDL), and some experimental results have been made available [6,8,39]. To validate our numerical framework for fibrous structures, we applied our methods to predict the cross-plane effective gas diffusion coefficient in dry fibrous materials and compared the results with the available experimental data. In our predictions, we assumed the fibers are straight in length with fixed diameter and random in position. The seed distribution probability s_d is chosen to produce the aimed porosity of the reconstructed fibrous structure. The lattice resolution for the fiber diameter is adopted as $\delta_x = d$ for two reasons: (***i***) the numerical model of a squared cross-section with a side length of one lattice step is closest to the realistic circular cross-section of cylindrical fiber; (***ii***) it has been verified in our previous work [24,26] that $\delta_x = d$ is sufficiently refined for modeling diffusion process in fibrous materials. The length of the fiber is assumed as the side length of the computational domain $l = 80\ \delta_x$, i.e. the growth of the fiber almost ends at the boundary of the domain. To capture

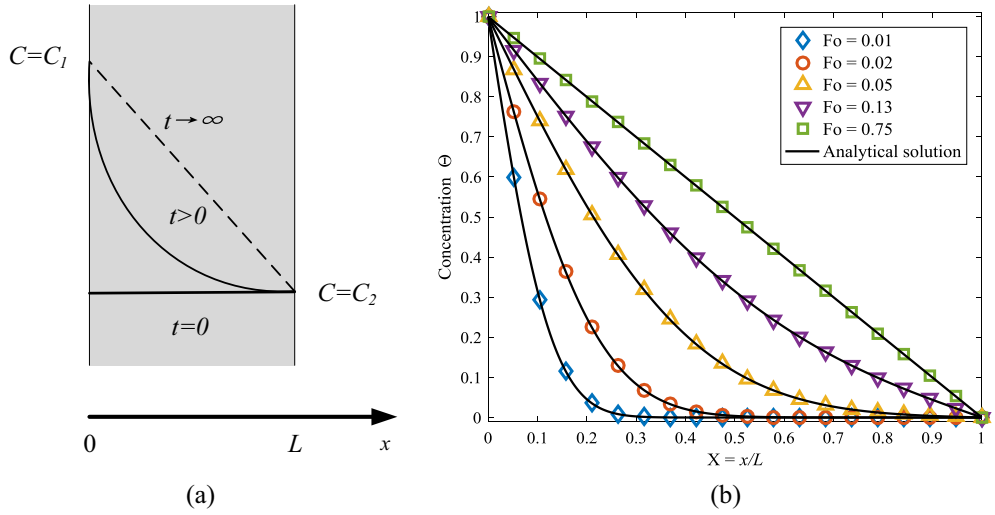

Fig. 6. Comparison of results from LBM simulations with the analytical solution: (a) Schematic for the one-dimensional transient gas diffusion problem; (b) the dimensionless concentration distribution at different dimensionless instants (Fo). The symbols represent the LBM results, while the solid lines represent the analytical solution Eq. (12).

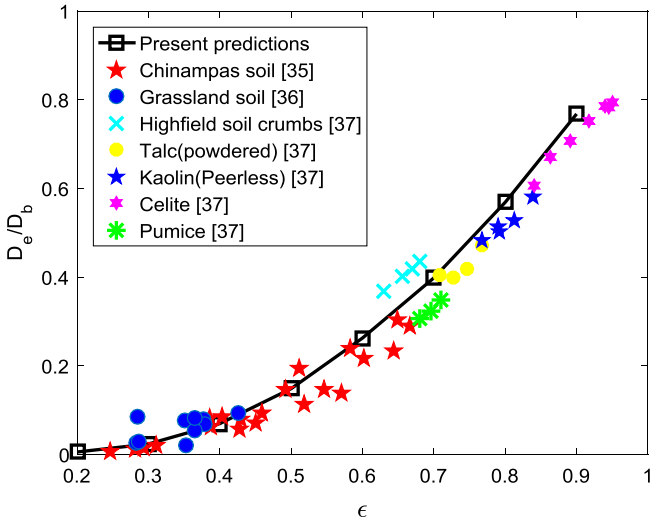

Fig. 7. Comparision of the effective gas diffusion coefficient between our simulations and the experimental data for granular structure. The solid line with squares is our numerical prediction using $s_d = 0.01$, whereas other symbols are from different experiments [35–37].

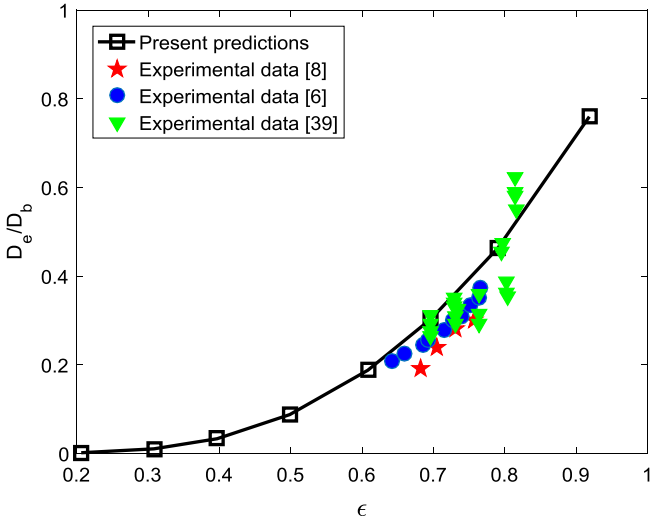

Fig. 8. Comparision of the cross-plane effective gas diffusion coefficient between the present simulations and experimental data for fibrous materials. The solid line with squares represent the present numerical prediction, whereas other symbols are the experimental data for GDL in the literature [6,8,39]. In our numerical modeling, the parameters for reconstructing microstructures are $d = \delta_x$, $l = 80\ \delta_x$, $\phi_{\text{lim}} = 5°$ and $\theta_{\text{lim}} = 180°$. The cross-plane direction represents the z direction perpendicular to the x-y plane (c.f. Fig. 1).

the highly anisotropic features of the GDL, we give the orientation angle limits as $\phi_{\text{lim}} = 5°$ and $\theta_{\text{lim}} = 180°$ (isotropic in the in-plane direction). Note that $\phi_{\text{lim}} = 0°$could predict nearly the same results as $\phi_{\text{lim}} = 5°$. A finite small value is adopted to be consistent with the real situation where slight fluctuations of the out-of-plane orientation angle are observed in the SEM picture of the GDLs [6,8]. The comparison of cross-plane gas effective diffusion coefficient versus porosity for dry fibrous materials is made in Fig. 8. A good agreement is obtained between the present numerical prediction and the experimental data, which indicates that our numerical framework works well for gas diffusion in such fibrous materials.

4. Results and discussions

The numerical model has been well established and validated as described above. In this section, a series of parametric studies will be carried out for a given fibrous system to examine the influences on the system behaviors of all the important parameters included in the model.

4.1. The effects of liquid saturation

In a porous medium, it is almost inevitable that the material will interact with surrounding moisture so that water, in either liquid or gaseous state, will penetrate into the structure to form a part of the system. Consequently the system properties will become a function of water saturation S, defined as the ratio between the volume fraction of liquid water and the porosity of the system [4]. In our numerical framework, we can reconstruct a fibrous microstructure with water partially saturated as described in Section 2.1, and demonstrated in Fig. 3(b). The reconstruction of fibrous structure is the same as that in Section 3.3. A lattice Boltzmann solution of the corresponding diffusion equations Eqs. (1) and (2) produces the effective diffusion coefficient of gas in porous materials as a function of water saturations. Since the effective gas diffusion coefficient of the un-saturated porous

material becomes negligibly small at the water saturation larger than a threshold value S_{th}, we merely consider a series of S smaller than S_{th} in the simulation. The present numerical results are displayed in Fig. 9, where a dimensionless relative diffusion coefficient R_D is defined as the ratio of the actual cross-plane effective gas diffusivity D_e to its value in dry conditions $D_{e,dry}$, i.e. $R_D = D_e/D_{e,dry}$. It is seen that the predicted relative gas diffusion coefficient decreases with the water saturations S, in good agreement with the experimental data in partially saturated GDLs made of hydrophobic carbon papers by Utaka et al. [5], where the threshold saturation value is about 0.6–0.7. One can easily envision that it is more difficult for gas to pass through a medium with higher water saturation. In turn, this also shows that our mesoscopic approach is still available for partially saturated cases.

As is stated above, in partially-saturated porous media, the effective gas diffusion coefficient is dependent on both porosity and saturation. The most popular formula for the effective diffusion coefficient in terms of porosity and saturation is commonly expressed as [4,39]:

$$\frac{D_e}{D_b} = f(\varepsilon)g(S) \tag{13}$$

where $f(\varepsilon)$ is a function of porosity and $g(S)$ is a function of water saturation, with an implicit assumption that there is no cross-coupling effect between both. In history, Eq. (13) originated in the empirical models for effective electrical conductivity of porous materials. As early as in 1873, Maxwell proposed an empirical correlation to describe the electrical conductivity of an electrolyte containing nonconducting dispersions in terms of the volume fraction of the dispersion particles [40]. Since then considerable efforts were devoted to the study on electrical transport properties of porous materials. One of the well-known relations is Archie's equation in petrophysics [41], which relates the effective electrical conductivity of sedimentary rock to its porosity and brine saturation as a product of the power term of them. Several more specific forms have been proposed for Eq.(13) [3,22,39]; however most of the theoretical models are restricted to simple and regular system geometries with no microstructure details at all, whence the parameters in the empirical models have to be determined case by case. For example, a common form for the saturation function $g(S)$ was given as [4,39]:

$$g(S) = (1 - S)^n \tag{14}$$

where n is the fitting parameters. Through analyzing the present numerical results, it is found that $n \cong 3$ is more suitable for hydrophobic structure, with the coefficient of determination $R^2 = 0.994$. Fig. 10 shows the prediction of the saturation function Eq. (14) in comparison to the present modeling results and two series of experimental data. The good agreement infers that such a simple saturation function Eq. (14) is capable of providing a good prediction in engineering practice without complex computations.

4.2. Morphology effects of isotropic microstructures

The microstructure morphology of porous media has been demonstrated to have significant effects on effective transport properties, such as in thermal and electrical conductivities [25], and effective permeability of fluid flow [42,43]. The same issue on the effective diffusion coefficient is investigated here by comparing between the granular and fibrous systems. To have a consistent comparison, we assume both systems are isotropic, i.e., system properties are direction independent. Therefore in reconstructing the granular structure, the directional growth rate D_i is fixed at each direction; while for fibrous structure, there is no orientation limit for fibers. All the elements are randomly distributed in the domain space. The calculated effective gas diffusion coefficients against the

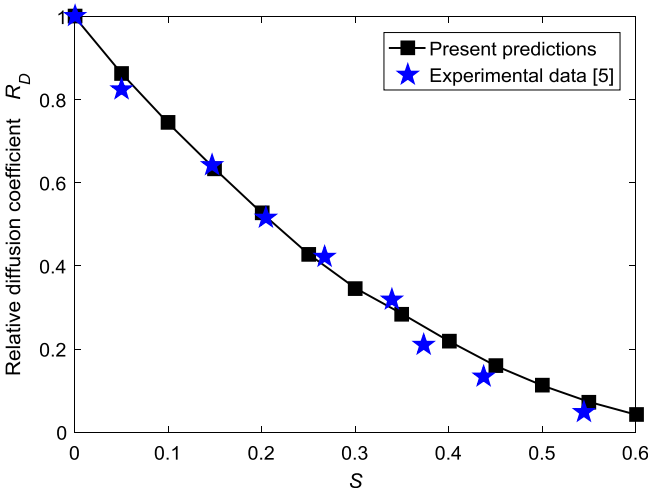

Fig. 9. Relative diffusion coefficient of partially saturated GDLs versus water saturation S. The solid line with squares represent the present numerical results, whereas the star symbols represent the experimental data of GDLs made of carbon papers [5].

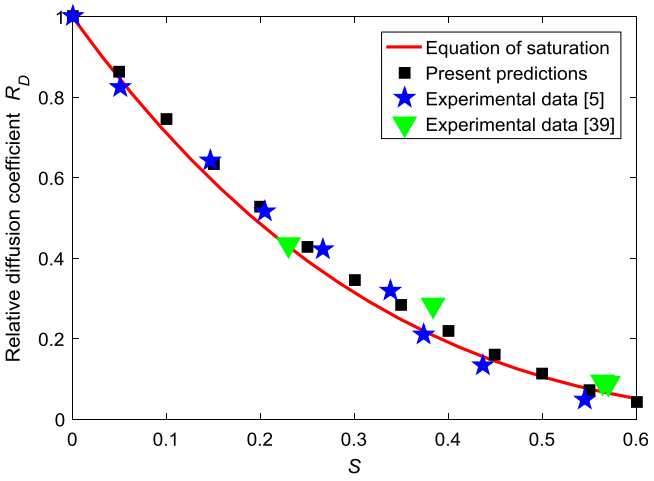

Fig. 10. Relative diffusion coefficient versus water saturation S for the partially-saturated porous media: the solid line represent the prediction by the empirical equation of saturation Eq. (14) with $n = 3$, the solid squares represent the present numerical results, whereas the star and triangle symbols represent the experimental data [5,39].

porosity are shown in Fig. 11(a) for the two systems, with no available experimental data in public literature for comparison. It is a bit surprising that, distinctive from the results for other transport properties, the gas diffusion in porous media seems to be insensitive to the structure morphology as inferred by the nearly coincidence between the two curves. It may be beneficial as this implies that any established empirical correlations in diffusion could be shared at least, between granular and fibrous systems. However, when the corresponding specific surface area for the two different morphologies is evaluated, a significant distinction between them is found, as shown in Fig. 11(b). This means that our predictions in Fig. 11(a) are only applicable for a pure Fickian-type gas diffusion process. According to Milligen et al. [44], the validity of Fick's Law requires that all the diffusion particles are non-interacting, going through a homogeneous medium and in the absence of external forces. When for example some multi-physic-chemical reactions on surfaces, such as adsorption or desorption, are involved, the morphology of structure will impact the gas diffusion properties significantly.

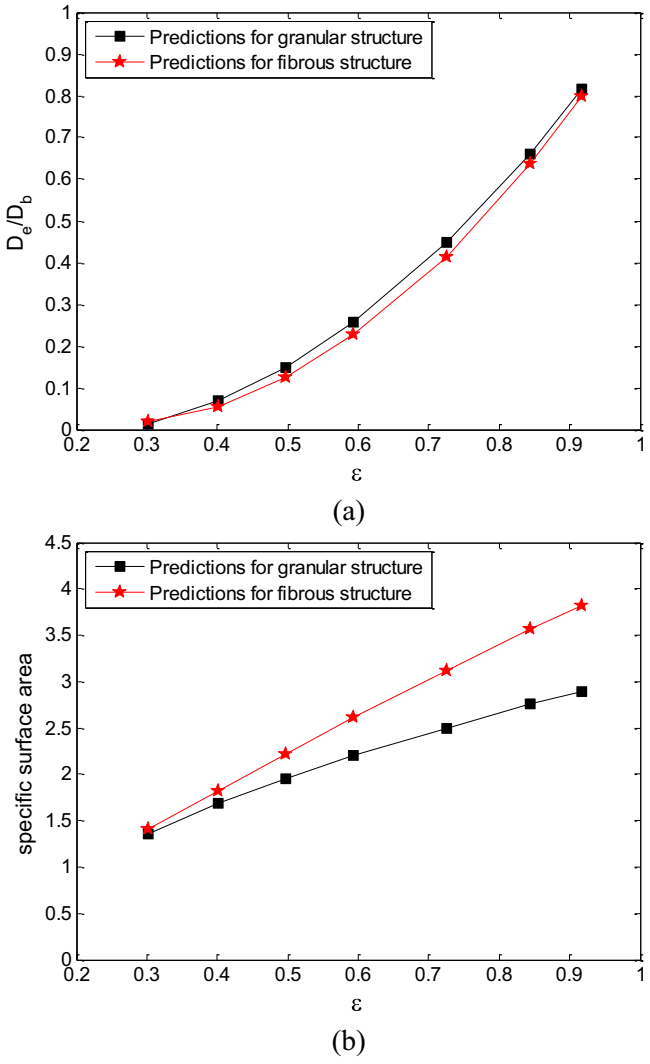

Fig. 11. Morphology effects of isotropic microstructure on (a) effective diffusion coefficient and (b) specific surface area versus porosity. The solid line with squares represent the granular structure whereas the solid line with stars represent the fibrous structure.

4.3. Orientation angle effects

In actual applications, the original microstructural isotropy of fibrous materials is usually lost in one or more directions due to the reinforcement or layering operations during manufacturing. The layering effect will be discussed in Section 4.4. The reinforcement is to force the fibers to re-orientate within certain angle limit ($\phi_{\rm lim}$, $\theta_{\rm lim}$), and a smaller orientation angle limit means a stronger anisotropy of structure. The resistance of gas diffusion along the fibers direction is smaller than that across the fibers direction. Thus we define the direction along the longitudinal direction of the system as the in-plane direction, and the other normal direction as the cross-plane direction. In this work, we use the difference of the effective gas diffusion coefficients between the in-plane and cross-plane directions to characterize the anisotropy of microstructure quantitatively.

Fig. 12 shows the effective gas diffusion coefficients of fibrous materials in different directions when $\phi_{\rm lim}$ = 5° and $\theta_{\rm lim}$ = 180° (isotropic in *x*-*y* plane). As expected, the in-plane diffusion coefficient is larger, often significantly, than the cross-plane value at the same porosity. The corresponding result for the completely isotropic case $\phi_{\rm lim} = \theta_{\rm lim} = 180^\circ$ is also considered and compared, and found

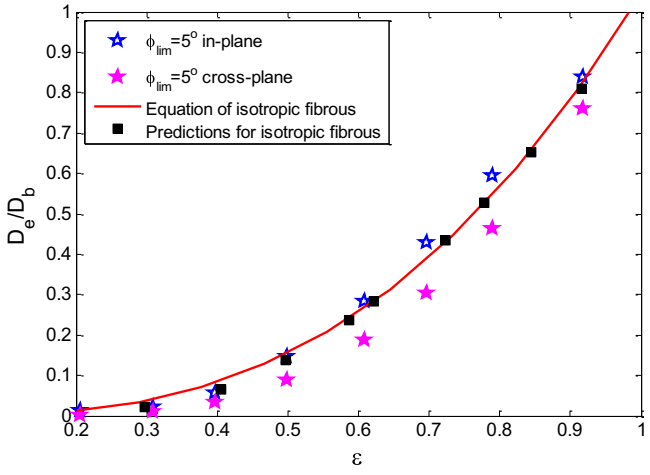

Fig. 12. The anisotropic effective gas diffusion coefficients verus porosity of fibrous media: the solid squares represent the present numerical results for isotropic structure, the blue and magenta stars represent the present in-plane and cross-plane numerical results respectively for anisotropic structure with $\phi_{\rm lim}$ = 5° and $\theta_{\rm lim}$ = 180° (isotropic in *x*-*y* plane), whereas the solid line represent the fitting curve. The in-plane direction represents the direction along *x*-*y* plane, whereas the cross-plane direction represents the *z* direction perpendicular to the *x*-*y* plane (c.f. Fig. 1).

to fall in between the in-plane and cross-plane ones. In other words, increasing the fiber orientation can enhance the gas diffusion coefficient along that direction. Furthermore, the effective gas diffusion coefficient of isotropic structures is often estimated using a power function of porosity as $D_{\rm e}/D_{\rm b} \equiv g(\varepsilon) = a\varepsilon^n$ [4]. Here we fit the simulation results for isotropic structure firstly to arrive at a = 1.05 and n = 3 within acceptable accuracy, as displayed as the solid line in Fig. 12.

For anisotropic fibrous structures with different fiber orientation angle limits, we propose an empirical correlation function:

$$\frac{D_{\rm e}}{D_{\rm b}} = g(\varepsilon)\chi(\phi_{\rm lim}) \tag{15}$$

where $g(\varepsilon)$ and $\chi(\phi_{\rm lim})$ are separately functions of porosity and orientation angle limit, again assuming no cross-coupling effect between them. Through carefully fitting a series of simulation results for the fiber orientation angle limit $\phi_{\rm lim}$ between 0° and 180°, a correlation of effective gas diffusion coefficients is provided as:

$$\frac{D_{\rm e}}{D_{\rm b}} = \begin{cases} a\varepsilon^n[\sin(\phi_{\rm lim}/2)]^{0.06} & {\rm cross-plane} \\ a\varepsilon^n[\sin(\phi_{\rm lim}/2)]^{-0.03} & {\rm in-plane} \end{cases}, \tag{16}$$

where a = 1.05 and n = 3, with the coefficient of determination R^2 being (0.976, 0.998). One may be concerned about whether the value of the expression Eq. (16) is within a reasonable range. Since the largest porosity of fibrous materials in practice usually remains some distance away from 1 (say, at most ~0.9), we have $a\varepsilon^n$ = 0.7655 when ε = 0.9. On the other hand, the larger in-plane value in Eq. (16) mathematically turns into infinity when $\phi_{\rm lim}$ approaches 0° due to the sine function term; but for a small finite value often in realistic highly anisotropic fibrous materials (such as GDLs in Section 3.3), for instance $\phi_{\rm lim} = 1^\circ$, we have $[\sin(\phi_{\rm lim}/2)]^{-0.03}$ = 1.1529. Even a combination of these two extreme situations gives a dimensionless effective gas diffusivity: 0.7655 × 1.1529 = 0.8825 still smaller than one. Therefore, the correlation Eq. (16) is feasible and available for most engineering applications. To demonstrate the effectiveness of Eq. (16) for estimating the anisotropic gas effective diffusion coefficients, we make a comparison of its prediction to the LBM numerical results at $\phi_{\rm lim}$ = 10° as an example in Fig. 13. Appreciably good agreements are achieved

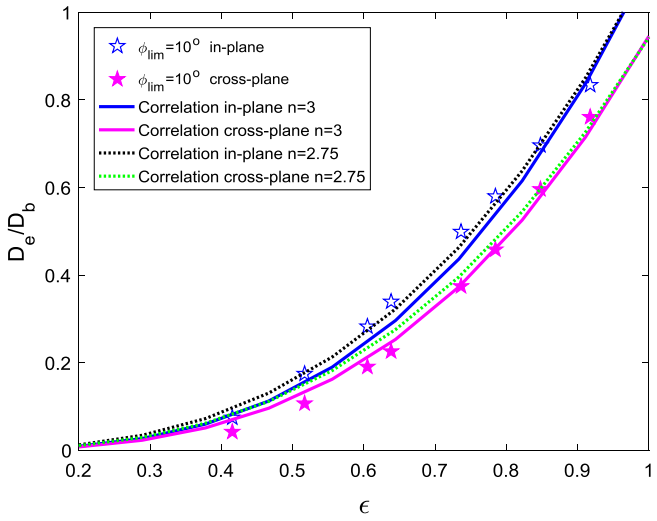

Fig. 13. The effective gas diffusion coefficients in in-plane and cross-plane directions of fibrous media versus porosity when $\phi_{lim} = 10°$ and $\theta_{lim} = 180°$. The symbols represent the present numerical results, whereas the lines represent the results by the correlation Eq. (16) with $a = 1.05$ and $n = 3$ or 2.75. The in-plane direction represents the direction along x-y plane, whereas the cross-plane direction represents the z direction perpendicular to the x-y plane (c.f. Fig. 1).

between the correlation and numerical results. We suggest that $n = 3$ for convenient engineering applications or $n = 2.75$ for more accurate predictions.

4.4. Layering structure effects

In applications for gas filtration [45], fibers are first formed individual layers and then a system is produced by laminating all the layers into one, as illustrated in Fig. 2(c). Such fiber layering will result in significant anisotropy in system properties. In our numerical framework, we reconstruct a layering fibrous structure by setting the z orientation angle limit $\phi_{lim} = 0°$ for fibers in the same layer, within each layer $\theta_{lim} = 180°$ to assure planar isotropy, and the layer-spacing δ varies from 0 to 2 lattice unit to examine the effect of layer-spacing δ on the system effective diffusion coefficient.

Fig. 14(a) shows the effective gas diffusion coefficients in the layered fibrous structures along different directions at different layer-spacing. We take the direction parallel to the layer (x-y plane) as the in-plane direction and the vertical (z) as the through-plane direction. It shows again that the effective diffusion coefficient at the in-plane direction is always higher than that at the through-plane direction. If we define a system anisotropy as the difference between the maximum and minimum values of D_e/D_b in a layered system of given spacing δ, then the anisotropy increases substantially with the increase of layer-spacing δ based on the results in Fig. 14(a). In other words, altering the layer-spacing δ can effectively adjust the anisotropic gas diffusivity, and it may be an important parameter for performance optimization in given applications.

Again, we propose a simple empirical correlation for engineering applications based on our modeling results for layering fibrous materials as:

$$\frac{D_e}{D_b} = K(\varepsilon, \delta) = \frac{A + B\varepsilon + C\delta}{1 + D\varepsilon + E\delta} \tag{17}$$

where A, B, C, D, E are empirical parameters to be specified through fitting the numerical results. Note Eq. (17) is similar to the one suggested by Zamel et al. [3]. The correlation is available for both the in-plane and through-plane directions, if with different fitting parameters. For extremely large layer-spacing value ($\delta \gg 1$) and large porosity ($\varepsilon \sim 1$), the system effective gas diffusivity may approach the bulk diffusivity, i.e. $D_e/D_b \simeq C/E$ would reach nearly unity. In other words, the value of parameter C should be almost identical to (nevertheless, slightly smaller than) the parameter E, as shown in the empirical parameters provided in Table 1 for

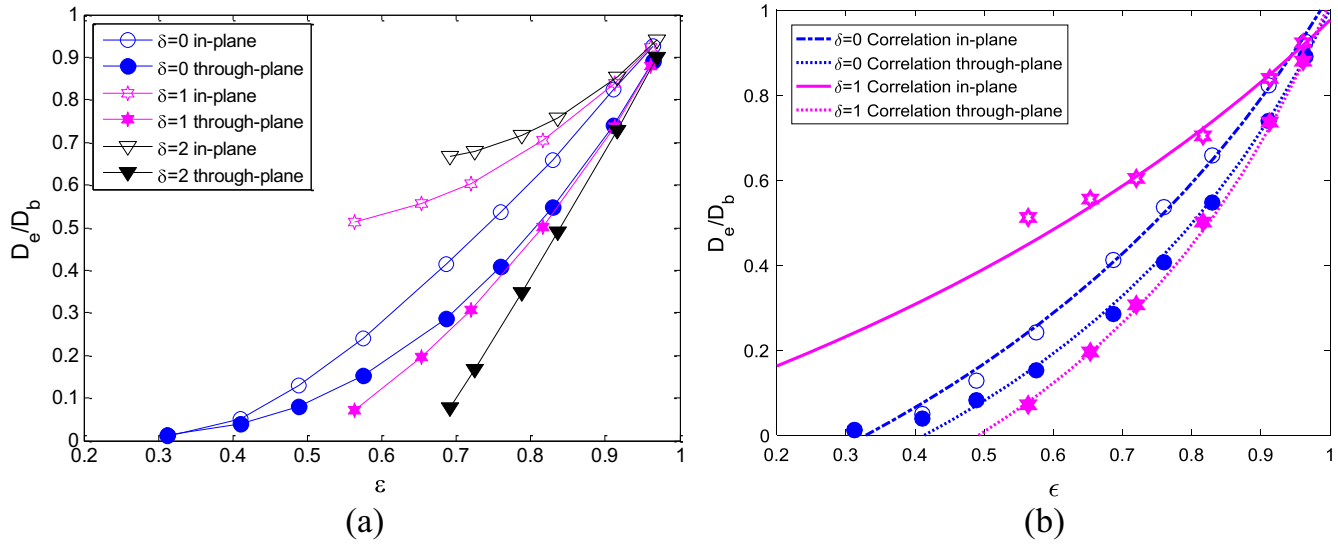

Fig. 14. The effective diffusion coefficients of layering structure v.s. porosity for different layer-spacing and different directions: (a) Results of present numerical simulation. (b) Prediction by the empirical correlation Eq. (17) in comparison to the simulation data. The in-plane direction denotes the direction along the laminated layer, whereas the through-plane direction denotes the direction perpendicular to the lamintated layer.

Table 1
The empirical parameters in the correlation Eq. (17) for layering fibrous materials.

Direction	A	B	C	D	E
In-plane	−0.24	0.72	0.29	−0.53	0.33
Through-plane	−0.27	0.65	−0.05	−0.62	−0.06

$0.3 < \varepsilon < 1$ with the coefficient of determination R^2 higher than 0.98. Consistent comparisons between the empirical correlation and the simulation results are shown in Fig. 14(b) at $\delta = 0$ and $\delta = 1$ as two examples.

5. Conclusions

Using the computational methods in this work, several typical gas diffusion processes with different conditions have been studied and some important conclusions are derived, including:

(i) The gas diffusion coefficient decreases with the water saturations in the system, i.e., it becomes more difficult for gas to pass through a medium with higher water saturation. The high agreement between our predictions and the existing experimental data indicates that our mesoscopic method is applicable for partially saturated cases. A simplified assumption in the present work is the ignorance of cross-coupling effect of the porosity and saturation on diffusion, which may be taken into account in future.

(ii) Different microstructural morphologies result in virtually the same effective gas diffusivity for a pure Fickian-type gas diffusion process, but yield an appreciable discrepancy in terms of the system specific surface area. Therefore, in the presence of other multi-physic-chemical phenomena, such as the adsorption or desorption at the surface, the morphology of structure will influence the system properties significantly.

(iii) Fiber orientation is the main cause of system anisotropy in diffusion, for clearly the resistance of gas diffusion along the fibers direction is smaller than that across the fibers direction. The available experimental data specifies there is no cross-coupling between ε and fiber orientation. Increasing the fiber orientation can enhance the gas diffusion coefficient in that direction. In a laminated structure, the anisotropy behavior increases substantially with elevated layer-spacing. In other words, altering the layer-spacing can effectively adjust the anisotropic gas diffusivity, and it could act as an important parameter for performance optimization.

Acknowledgments

This work is financially supported by the NSF grant of China (No. U1562217, 51321002), National Key Basic Research Program of China (No.2015CB250902), National Science and Technology Major Project on Oil and Gas (No.2017ZX05013001) and the PetroChina Innovation Foundation (2015D-5006-0201).

References

[1] E.L. Cussler, Diffusion: Mass Transfer in Fluid Systems, Cambridge University Press, 2009.
[2] B.A. Grzybowski, K.J. Bishop, C.J. Campbell, M. Fialkowski, S.K. Smoukov, Micro- and nanotechnology via reaction–diffusion, Soft Matter 1 (2) (2005) 114–128.
[3] N. Zamel, X. Li, J. Shen, Correlation for the effective gas diffusion coefficient in carbon paper diffusion media, Energy Fuels 23 (12) (2009) 6070–6078.
[4] J.H. Nam, M. Kaviany, Effective diffusivity and water-saturation distribution in single- and two-layer PEMFC diffusion medium, Int. J. Heat Mass Transf. 46 (24) (2003) 4595–4611.
[5] Y. Utaka, I. Hirose, Y. Tasaki, Characteristics of oxygen diffusivity and water distribution by X-ray radiography in microporous media in alternate porous layers of different wettability for moisture control in gas diffusion layer of PEFC, Int. J. Hydrogen Energy 36 (15) (2011) 9128–9138.
[6] G. Unsworth, L. Dong, X.G. Li, Improved experimental method for measuring gas diffusivity through thin porous media, AIChE J. 59 (4) (2013) 1409–1419.
[7] H.L. Penman, Gas and vapour movements in the soil: II. The diffusion of carbon dioxide through porous solids, J. Agric. Sci. 30 (04) (1940) 570–581.
[8] C. Chan, N. Zamel, X.G. Li, J. Shen, Experimental measurement of effective diffusion coefficient of gas diffusion layer/microporous layer in PEM fuel cells, Electrochim. Acta 65 (2012) 13–21.
[9] A. Kühne, H. Schack-Kirchner, E.E. Hildebrand, Gas diffusivity in soils compared to ideal isotropic porous media, J. Plant Nutr. Soil Sci. 175 (1) (2012) 34–45.
[10] D.H. Shou, J.T. Fan, F. Ding, Effective diffusivity of gas diffusion layer in proton exchange membrane fuel cells, J. Power Sources 225 (2013) 179–186.
[11] M.M. Tomadakis, S.V. Sotirchos, Ordinary and transition regime diffusion in random fiber structures, AIChE J. 39 (3) (1993) 397–412.
[12] D.A.G. Bruggeman, Calculation of various physics constants in heterogenous substances I Dielectricity constants and conductivity of mixed bodies from isotropic substances, Ann. Phys. 24 (7) (1935) 636–664.
[13] S. Li, L.J. Lee, J. Castro, Effective mass diffusivity in composites, J. Compos. Mater. 36 (14) (2002) 1709–1724.
[14] D. Shou, J. Fan, M. Mei, F. Ding, An analytical model for gas diffusion though nanoscale and microscale fibrous media, Microfluid. Nanofluid. 16 (1–2) (2014) 381–389.
[15] B.R. Bateman, J.D. Way, K.M. Larson, An apparatus for the measurement of gas fluxes through immobilized liquid membranes, Sep. Sci. Technol. 19 (1) (1984) 21–32.
[16] P. Gibson, H. Schreuder-Gibson, D. Rivin, Transport properties of porous membranes based on electrospun nanofibers, Colloids Surf. A 187–188 (2001) 469–481.
[17] J.M. LaManna, S.G. Kandlikar, Determination of effective water vapor diffusion coefficient in pemfc gas diffusion layers, Int. J. Hydrogen Energy 36 (8) (2011) 5021–5029.
[18] L. Hao, P. Cheng, Lattice Boltzmann simulations of anisotropic permeabilities in carbon paper gas diffusion layers, J. Power Sources 186 (1) (2009) 104–114.
[19] D. Froning, J. Brinkmann, U. Reimer, V. Schmidt, W. Lehnert, D. Stolten, 3D analysis, modeling and simulation of transport processes in compressed fibrous microstructures, using the Lattice Boltzmann method, Electrochim. Acta 110 (2013) 325–334.
[20] M.M. Tomadakis, S.V. Sotirchos, Effective diffusivities and conductivities of random dispersions of nonoverlapping and partially overlapping unidirectional fibers, J. Chem. Phys. 99 (12) (1993) 9820–9827.
[21] J. Becker, C. Wieser, S. Fell, K. Steiner, A multi-scale approach to material modeling of fuel cell diffusion media, Int. J. Heat Mass Transf. 54 (7–8) (2011) 1360–1368.
[22] N. Zamel, X. Li, Effective transport properties for polymer electrolyte membrane fuel cells – With a focus on the gas diffusion layer, Prog. Energy Combust. Sci. 39 (1) (2013) 111–146.
[23] M. Wang, J. Wang, N. Pan, S. Chen, Mesoscopic predictions of the effective thermal conductivity for microscale random porous media, Phys. Rev. E 75 (3) (2007) 036702.
[24] M. Wang, J. He, J. Yu, N. Pan, Lattice Boltzmann modeling of the effective thermal conductivity for fibrous materials, Int. J. Therm. Sci. 46 (9) (2007) 848–855.
[25] M. Wang, N. Pan, Predictions of effective physical properties of complex multiphase materials, Mater. Sci. Eng. R-Rep. 63 (1) (2008) 1–30.
[26] M. Wang, Q. Kang, N. Pan, Thermal conductivity enhancement of carbon fiber composites, Appl. Therm. Eng. 29 (2) (2009) 418–421.
[27] M. Wang, N. Pan, J. Wang, S. Chen, Mesoscopic simulations of phase distribution effects on the effective thermal conductivity of microgranular porous media, J. Colloid Interface Sci. 311 (2) (2007) 562–570.
[28] M. Wang, Q. Chen, Q. Kang, N. Pan, E. Ben-Nairn, Nonlinear effective properties of unsaturated porous materials, Int. J. Nonlinear Sci. Num. Simul. 11 (1) (2010) 49–56.
[29] J.D. Ramshaw, Self-consistent effective binary diffusion in multicomponent gas mixtures, J. Non-Equilib. Thermodyn. 15 (3) (1990) 295–300.
[30] J. Wang, M. Wang, Z. Li, A lattice Boltzmann algorithm for fluid–solid conjugate heat transfer, Int. J. Therm. Sci. 46 (3) (2007) 228–234.
[31] J. Wang, M. Wang, Z. Li, Lattice evolution solution for the nonlinear Poisson-Boltzmann equation in confined domains, Commun. Nonlinear Sci. Numer. Simul. 13 (3) (2008) 575–583.
[32] C. Xie, J. Wang, D. Wang, N. Pan, M. Wang, Lattice Boltzmann modeling of thermal conduction in composites with thermal contact resistance, Commun. Comput. Phys. 17 (04) (2015) 1037–1055.
[33] Q.S. Zou, X.Y. He, On pressure and velocity boundary conditions for the lattice Boltzmann BGK model, Phys. Fluids 9 (6) (1997) 1591–1598.
[34] A. Faghri, Y. Zhang, J.R. Howell, Advanced Heat and Mass Transfer, Global Digital Press, 2010.
[35] E. Ikkonen, N.E. García-Calderón, E. Stephan-Otto, A. Martínez-Arroyo, Difusión de gases en suelos de chinampas en la Ciudad de México, SJSS: Spanish, J. Soil Sci. 2 (3) (2012).
[36] A. Boon, J.S. Robinson, P.D. Nightingale, L. Cardenas, D.R. Chadwick, A. Verhoef, Determination of the gas diffusion coefficient of a peat grassland soil, Eur. J. Soil Sci. 64 (5) (2013) 681–687.
[37] J.A. Currie, Gaseous diffusion in porous media. Part 2. - Dry granular materials, Br. J. Appl. Phys. 11 (8) (1960) 318–324.
[38] Q. Ma, Z.Q. Chen, J. Shi, D. Li, Lattice Boltzmann modeling of VOC desorption and diffusion in porous materials VOC desorption and diffusion, Build. Environ. 72 (2014) 145–153.
[39] G.S. Hwang, A.Z. Weber, Effective-diffusivity measurement of partially-saturated fuel-cell gas-diffusion layers, J. Electrochem. Soc. 159 (11) (2012) F683–F692.

[40] J. Maxwell, A Treatise on Electricity and Magnetism, Clarendon Press, Oxford, 1873.
[41] G.E. Archie, The electrical resistivity log as an aid in determining some reservoir characteristics, Trans. AIME 146 (01) (1942) 54–62.
[42] S. Chen, X. He, V. Bertola, M. Wang, Electro-osmosis of non-Newtonian fluids in porous media using lattice Poisson-Boltzmann method, J. Colloid Interface Sci. 436 (2014) 186–193.
[43] M. Wang, Structure effects on electro-osmosis in microporous media, J. Heat Transfer 134 (5) (2012) 051020.
[44] B.P.v. Milligen, P.D. Bons, B.A. Carreras, R. Śanchez, On the applicability of Fick's law to diffusion in inhomogeneous systems, Eur. J. Phys. 26 (2005) 913–925.
[45] J. Wang, S.C. Kim, D.Y.H. Pui, Carbon nanotube penetration through a screen filter: numerical modeling and comparison with experiments, Aerosol Sci. Technol. 45 (3) (2011) 443–452.